Pressure Drop and Flow Pattern of Slush Nitrogen in a Horizontal Pipe

Yuye Jiang and Peng Zhang
Institute of Refrigeration and Cryogenics, Shanghai Jiao Tong University, Shanghai 200240, China

DOI 10.1002/aic.13927
Published online October 22, 2012 in Wiley Online Library (wileyonlinelibrary.com).

Slush nitrogen is a mixture of solid nitrogen particles and liquid nitrogen, and its flow characteristics in a horizontal pipe are investigated experimentally and theoretically in this study. Pressure drop of slush nitrogen is higher than that of subcooled liquid nitrogen due to the viscous and the mechanical frictions, and the dependence of pressure drop on the mean velocity varies under different flow conditions. The solid volume fraction distributions and the velocity throughout the pipe cross-section of slush nitrogen flow are investigated with the Eulerian–Eulerian multiphase approach incorporated with the kinetic theory of granular flow. The flow patterns of slush nitrogen are determined as the pseudo-homogeneous flow, the heterogeneous flow and the bedload flow from the experimental and numerical results. The relationship between the friction factor and the Reynolds number for slush nitrogen with various solid volume fractions is obtained by using the slush Reynolds number. © 2012 American Institute of Chemical Engineers *AIChE J,* 59: 1762–1773, 2013
Keywords: slush nitrogen, flow pattern, particle, fluid mechanics, hydrodynamics

Introduction

Slush nitrogen is a cryogenic slurry fluid containing solid nitrogen particles in liquid nitrogen and has multiple advantages over subcooled liquid nitrogen.[1] The temperature of slush nitrogen is 63 K, that is, the triple point of nitrogen, lower than that of subcooled liquid nitrogen, and can be kept stable until the solid melts completely. Slush nitrogen has higher cooling capacity, because it absorbs the latent heat of fusion when solid particles melts, which decreases the coolant consumption and the system size. More importantly, the generation of vapor bubbles is suppressed effectively due to the presence of the solid particles, which can prevent the sudden increase of the local temperature, and therefore, the stability of the cooling system is highly improved. Hence, slush nitrogen is considered as a better coolant for high-temperature superconductive magnets and devices than subcooled liquid nitrogen. The investigation of cryogenic slurries, including slush nitrogen, slush hydrogen, and slush oxygen, and so forth, started in 1960s[2] and mainly focused on slush production and storage, measurement technology, and the flow and heat transfer characteristics in the pipelines from the experimental and theoretical aspects.

When slush nitrogen flows in a horizontal pipe, the pressure drop is slightly higher than that of subcooled liquid nitrogen under the same condition, and it increases with the solid volume fraction at the same velocity. But the influence of the solid volume fraction vanished at the mean velocity of about 3.5 m/s,[3] and it is considered that solid particles are capable of suppressing the turbulence of the flow, so that the effective viscosity of slurry may decrease under certain conditions. And the pressure drop reduction at higher velocity has been reported,[4,5] because the turbulence generation near the pipe wall is suppressed due to the migration of solid particles toward the pipe center, and the pseudo-homogeneous flow pattern is considered to occur. Except in the pressure drop reduction region, the pressure drop of slush nitrogen increases with the increase of the mean velocity when the solid volume fraction is 4–40% and the mean velocity is 0.2–5.9 m/s,[3,5] which is very different from the typical slurry flow. In general, slurry flows in a horizontal pipe are more complicated, because the motion of the solid particles is affected by several forces. The gravity perpendicular to the flow direction tends to deposit the particles at the bottom of the pipe. And some dispersive actions, such as turbulent diffusion, particle contact, particle–wall interaction, Brownian motion, and surface forces, and so forth, tend to make the particles uniformly suspended in the liquid, and the combined influence of these forces on slurry flow depends on the flow conditions, thus, resulting in the significantly various behavior of slurry flow. The slurry flows in a horizontal pipe are generally categorized into four flow patterns: homogeneous flow, heterogeneous flow, moving-bed flow, and stationary-bed flow according to the particles distribution over the pipe cross-section.[6] The flow pattern is influenced by many variables, including pipe dimension, properties of two phases, flow velocity, solid volume fraction, and so forth, and the flow behavior and the associated mechanisms generally vary with the flow patterns. Despite the small density difference between the solid and liquid phases in slush nitrogen, the different flow patterns were evidenced in the visualization results in the experiments,[7] but these flow patterns cannot be distinguished from the pressure drop of slush nitrogen like the conventional slurries.

Correspondence concerning this article should be addressed to P. Zhang at zhangp@sjtu.edu.cn.

On the theoretical study of slurry flow, two modeling approaches, the Eulerian–Lagrangian and the Eulerian–Eulerian approaches, are generally applied, and the selection of the approach depends on several factors such as particle size, volume fraction, and Stokes number. Ishimoto and Ono[8] used the Eulerian–Lagrangian model to investigate the slush nitrogen flow in the horizontal pipes, and the developed model was successfully used for the different pipes due to the application of the generalized curvilinear coordinates system. In the Eulerian–Lagrangian model, the forces acting on the particles are all considered, and the motion equations are solved for each particles, so that the particle-level phenomena can be reasonably predicted.[9] The Eulerian–Lagrangian approach gives satisfactory results in the case of dilute slurry flow with small particles and low Stokes number, but it is considered inappropriate for the concentrated slurry flows, because the dominant flow mechanism changes in such cases. In addition, the computing expense is significantly increased because of the large amount of the particles. Ohira et al.[10] applied the Eulerian–Eulerian approach to slush nitrogen flow, and some flow behaviors such as pressure drop and the velocity distribution on the cross-section of the pipe were successfully predicted, but the particle-free region that was mentioned in their experimental study was not obtained in the modeling. Hence, another Eulerian–Eulerian multiphase model based on the kinetic theory of granular flow was developed for slush nitrogen flow with a wide range of solid volume fractions.[11] The solid phase is assumed as a continuous phase, interpenetrating and interacting with the fluid phase within each control volume, and the continuity and momentum equations are solved for both phases, and the motion of particles is modeled using the kinetic theory of granular flow that was developed from the kinetic theory of gases.[12–14] The Eulerian–Eulerian multiphase model incorporated with the kinetic theory of granular flow is capable of giving satisfactory results of various slurry flows using appropriate parameters.[15–17] As the properties of slush nitrogen, especially the properties of solid nitrogen particles, are not clearly understood, some models such as the turbulence model, the drag model, and some parameters appropriate to slush nitrogen are determined by the sensitivity analysis. And the accuracy of the developed model has been validated with the experimental results of slurry and slush nitrogen flows from the literature.

Although many investigations have been conducted, the flow characteristics of slush nitrogen are still not understood sufficiently, especially for the difference of pressure drop and flow patterns between slush nitrogen and the conventional slurries. In this study, the flow characteristics and the associated mechanism of slush nitrogen in a horizontal pipe are investigated experimentally and theoretically. A series of experiments are carried out to investigate the effects of the mean velocity and the solid volume fraction on the pressure drop of slush nitrogen, and the corresponding flow patterns are clarified. Meanwhile, the computational fluid dynamics (CFD) is conduced to study the detailed flow behavior and the mechanism of slush nitrogen. The Eulerian–Eulerian multiphase model incorporated with the kinetic theory of granular flow developed in the previous study is applied to model the flow of slush nitrogen under the same conditions as in the experiments, and the detailed flow behavior of slush nitrogen, such as the distributions of solid particles and the velocity are obtained and discussed.

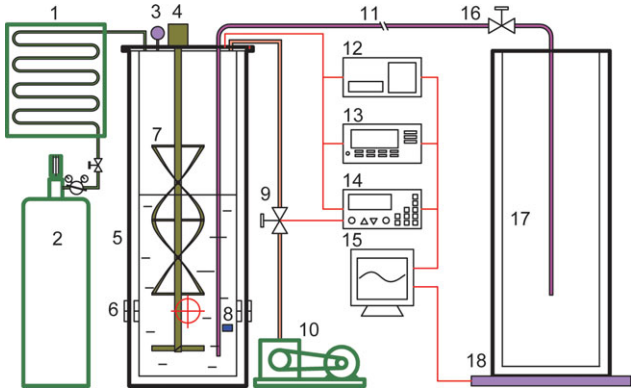

Figure 1. Schematic diagram of the experimental apparatus—1: heat exchanger; 2: helium gas cylinder; 3: pressure sensor; 4: electric motor; 5: production dewar; 6: observation windows; 7: agitator; 8: densimeter; 9: exhaust throttle valve; 10: vacuum pump; 11: test pipe; 12: LCR meter; 13: data acquisition device; 14: pressure controller; 15: computer; 16: cryogenic valve; 17: receive dewar; 18: electric balance.

[Color figure can be viewed in the online issue, which is available at wileyonlinelibrary.com.]

Experimental Apparatus and Procedure

Figure 1 shows the schematic illustration of the experimental apparatus in this study, which contains two parts: the slush nitrogen production device and the pipe for slush nitrogen flow. First, slush nitrogen is produced by the freeze–thaw method in the production dewar, and the maximum pumping speed of the vacuum pump is 8 L/s, and the time of the freeze and thaw cycles are 10 and 5 s, respectively. When solid nitrogen particles are generated, the particles are observed from the side observation windows. The particle size is determined to be about 1.0 mm by comparing with the thickness of the blades and the densimeter, and the value of 1.0 mm is very close to the result reported previously.[3,5] When the solid volume fraction of slush nitrogen reaches the prescribed value, the production is stopped and the production dewar is pressurized with helium gas that is precooled by liquid nitrogen in the heat exchanger to improve the stability of the pressure in the production dewar and also to reduce the heat carried into the dewar by the helium gas. The pressure in the receive dewar is kept at 0.1 MPa, and the pressure in the production dewar is changed in the range of 0.13–0.2 MPa to reduce the risk of breaking the observation windows made of glass. Then, the pressure difference is formed between the production dewar and the receive dewar and drives the slush nitrogen to flow through the test pipe, and the flow velocity can be controlled by both the pressure difference between two dewars and the cryogenic valve installed at the downstream of the pipeline. The test pipe made of stainless steel has the inner diameter of 10.0 mm and is composed of the entrance section and the test section. The entrance section has the length of 0.8 m in the horizontal part and is located upstream of the test section to eliminate the effect of the elbow of the tube and also to ensure that the flow of slush nitrogen is fully developed. The test section has the length of 1.0 m, and the flow behavior of slush nitrogen is examined in this section. The entire test pipe is protected by the vacuum thermal

insulation structure to reduce the heat leakage from the outside during the experiments.

The density of slush nitrogen is determined by the capacitance-type densimeter system consisting of the densimeter, the inductance capacitance resistance (LCR) meter, and the double-shielded cables. The bulk shielding technology is applied to improve the performance of the densimeter system, and the measuring accuracy is within $\pm 0.25\%$ for slush density.[18] The mean velocity of slush nitrogen is calculated from the weight change of the receive dewar that is measured by the electric balance with the measuring accuracy within $\pm 0.1\%$, and the pressure drop of slush nitrogen is measured by the differential pressure transducer installed between the inlet and outlet of the test section, and the measuring accuracy is less than $\pm 0.5\%$. The temperature of the fluid in the production dewar is measured by the Rh–Fe resistance thermometers that are precalibrated and have the accuracy within ± 0.1 K. The signals of the temperature and pressure are both collected by the data acquisition device and then stored in the computer together with the capacitance measured by the LCR meter.

Mathematical Modeling

The flow behavior of slush nitrogen in a horizontal pipe with the inner diameter of 10.0 mm is numerically investigated with the Eulerian–Eulerian multiphase model incorporated with the kinetic theory of granular flow. The slush flow in the modeling is turbulent, because the Reynolds number is generally higher than 10^4, and the solid nitrogen particles are assumed as the smooth, inelastic, and spherical particles with the same size of 1.0 mm. The mathematical models used in the study are presented in Table 1,[11] where the subscript $i = \mathrm{l}$ or s, respectively, and q is the other phase relative to the phase i.

In the Eulerian–Eulerian multiphase model, the dispersed phase is considered as a continuous fluid, and the continuity and momentum equations are solved for both the liquid and the solid phases. The last three terms on the right-hand side of the momentum equation given by Eq. 2 are the interphase forces: the drag force, the lift force, and the virtual mass force. The drag force is one of the most important forces between two phases, and the drag coefficient β is calculated by the Gidaspow model[19] as shown by Eqs. 5–7. When a particle moves in a liquid with the velocity gradient, the pressure gradient will form over the particle, pushing the particle toward the region with the higher velocity. This force is known as the lift force, which is found more significant for the larger particles like solid nitrogen particles. And the lift coefficient C_{L} in the momentum equations is taken as 0.25 for spherical particles.[20] The virtual mass force acting on the particles is created when the particles accelerate relative to the liquid phase and the virtual mass coefficient $C_{\mathrm{VM}} = 0.5$.[21] As the large solid particles in slush nitrogen tend to increase the turbulence intensity, the per-phase k–ε turbulence model, where the equations of k and ε are solved for both solid and liquid phases, is applied in this study to consider the influence of solid particles on the liquid comprehensively. And the empirical constants in the model are $C_{\mu} = 0.09$, $C_{1\varepsilon} = 1.42$, $C_{2\varepsilon} = 1.92$, $C_{3\varepsilon} = 1.2$, $\sigma_{\mathrm{k}} = 1$, $\sigma_{\varepsilon} = 1.3$, $\sigma_{\mathrm{sl}} = 0.75$, respectively.

The motion of solid particles is modeled by the kinetic theory of granular flow where the inelastic collisions among the particles and between the particles and the pipe wall are considered. The fluctuating motion of solid particle is described by the granular temperature $\Theta_{\mathrm{s}} = \frac{1}{3}\overline{u_{\mathrm{s}}' u_{\mathrm{s}}'}$, where u_{s}' is the fluctuating velocity of the particles. The conservation equation of solid fluctuating energy and the constitutive equations are given by Eqs. (12)–(18).[14,19] $\alpha_{\mathrm{s,max}}$ is the maximum solid volume fraction, the value of which depends on the particle shape, size distribution, and the interactions between particles. In this study, the proper maximum solid volume fraction for slush nitrogen is evaluated in the experiment. After slush nitrogen is generated in the production dewar, the agitator is stopped and solid particles deposit randomly at the bottom of the dewar and the solid volume fraction is measured by the capacitance-type densimeter. The results of several repeated experiments indicate that maximum solid volume fraction of slush nitrogen is in the range of 0.48–0.54, obviously smaller than 0.63, which is the maximum volume fraction for the random packing of spherical particles. This is because solid nitrogen particles created by the freeze-thaw method in the experiment generally have irregular shapes and cannot deposit as closely as the spherical particles. Considering the assumption of the spherical particles in the simulation, the maximum solid volume fraction $\alpha_{\mathrm{s,max}}$ is taken as 0.52, which is the value for the simple cubic packing of the monodispersed spherical particles.[22]

Initially, there are no particles in the pipe, and the velocity of the liquid phase is zero. The velocities of two phases and the solid volume fraction are specified uniformly at the inlet, and the turbulence intensity I is calculated by the correlation $I = 0.16\ \mathrm{Re}^{-1/8}$. The pressure outlet condition is applied at the outlet. The no-slip condition is used for the liquid phase and the Johnson–Jackson wall boundary condition[23] is adopted for solid phase at the pipe wall. Specularity coefficient is taken as $\phi = 0.02$, representing that 2% of the tangential momentum is lost in the particle–wall collisions.[24]

The three-dimensional modeling of slush nitrogen flow is carried out using the commercial CFD software FLUENT 12.0 in this study, and the pressure–velocity coupling correlation is solved by the phase-coupled SIMPLE algorithm that is an extension of the SIMPLE algorithm to the multiphase flows. In the modeling, the diameter of the pipe is $D = 10.0$ mm, the same as that in the experiment, and the pipe length L is taken as 700.0 mm, which has been proved sufficient to ensure that the fully developed flow results can be obtained for all cases. The hexahedral mesh is utilized, and the grid is uniform along the pipeline and is refined appropriately in the near-wall region on the cross-section of the pipe. The grid-independent investigation is first conducted to avoid the high computation error or even unreasonable results arising from a coarse grid scheme. It is found that when the grid number is higher than 308,000, the further refinement of the mesh will not change the modeling results obviously, indicating the mesh size is fine enough for the modeling. The time step is 0.0001 s, and the solution is assumed to converge when the convergence criterion is lower than 1.0×10^{-4}. The multiphase model used here has been validated with a series of experimental results of slurries flow and slush nitrogen flow from the literature, and the details have been given in Ref. 11.

Results and Discussion

Flow of subcooled liquid nitrogen

The flow of subcooled liquid nitrogen at the triple point (63 K) in the horizontal pipe with the inner diameter of 10.0 mm is examined to verify the accuracy of the experimental

Table 1. Mathematical Model

Continuity equations

$$\frac{\partial}{\partial t}(\alpha_i\rho_i) + \nabla\cdot(\alpha_i\rho_i\boldsymbol{U}_i) = 0 \tag{1}$$

Momentum equations

$$\frac{\partial}{\partial t}(\alpha_i\rho_i\boldsymbol{U}_i) + \nabla\cdot(\alpha_i\rho_i\boldsymbol{U}_i\boldsymbol{U}_i) = -\alpha_i\nabla P + \nabla\cdot\boldsymbol{\tau}_i + \alpha_i\rho_i\boldsymbol{g} + \left[\beta(\boldsymbol{U}_q-\boldsymbol{U}_i) - C_{\mathrm{L}}\alpha_{\mathrm{s}}\rho_{\mathrm{l}}(\boldsymbol{U}_q-\boldsymbol{U}_i)\times(\nabla\times\boldsymbol{U}_{\mathrm{l}}) + C_{\mathrm{VM}}\alpha_{\mathrm{s}}\rho_{\mathrm{l}}\left(\frac{D_q\boldsymbol{U}_q}{Dt}-\frac{D_i\boldsymbol{U}_i}{Dt}\right)\right] \tag{2}$$

$$\boldsymbol{\tau}_l = \alpha_{\mathrm{l}}\mu_{\mathrm{l,eff}}\left[\nabla\boldsymbol{U}_{\mathrm{l}} + (\nabla\boldsymbol{U}_{\mathrm{l}})^T\right] - \frac{2}{3}\alpha_{\mathrm{l}}\mu_{\mathrm{l,eff}}(\nabla\cdot\boldsymbol{U}_{\mathrm{l}})\mathbf{I} \tag{3}$$

$$\boldsymbol{\tau}_s = \alpha_{\mathrm{s}}\mu_{\mathrm{s}}\left[\nabla\boldsymbol{U}_{\mathrm{s}} + (\nabla\boldsymbol{U}_{\mathrm{s}})^T - \frac{2}{3}(\nabla\cdot\boldsymbol{U}_{\mathrm{s}})\mathbf{I}\right] + (-P_{\mathrm{s}} + \lambda_{\mathrm{s}}\nabla\cdot\boldsymbol{U}_{\mathrm{s}})\mathbf{I} \tag{4}$$

Gidaspow drag model

$$\beta = \begin{cases} \frac{3}{4}C_{\mathrm{D}}\frac{\alpha_{\mathrm{s}}\alpha_{\mathrm{l}}\rho_{\mathrm{l}}|\boldsymbol{U}_{\mathrm{l}}-\boldsymbol{U}_{\mathrm{s}}|}{d_{\mathrm{p}}}\alpha_{\mathrm{l}}^{-2.65} & (\alpha_{\mathrm{l}} > 0.8) \\ 150\frac{\alpha_{\mathrm{s}}^2\mu_{\mathrm{l}}}{\alpha_{\mathrm{l}}d_{\mathrm{p}}^2} + 1.75\frac{\rho_{\mathrm{l}}\alpha_{\mathrm{s}}|\boldsymbol{U}_{\mathrm{l}}-\boldsymbol{U}_{\mathrm{s}}|}{d_{\mathrm{p}}} & (\alpha_{\mathrm{l}} \le 0.8) \end{cases} \tag{5}$$

$$C_{\mathrm{D}} = \begin{cases} 0.44 & (Re_{\mathrm{p}} > 1000) \\ \frac{24}{Re_{\mathrm{p}}}\left[1 + 0.15Re_{\mathrm{p}}^{0.687}\right] & (Re_{\mathrm{p}} \le 1000) \end{cases} \tag{6}$$

$$Re_{\mathrm{p}} = \frac{\alpha_{\mathrm{l}}\rho_{\mathrm{l}}|\boldsymbol{U}_{\mathrm{l}}-\boldsymbol{U}_{\mathrm{s}}|d_{\mathrm{p}}}{\mu_{\mathrm{l}}} \tag{7}$$

Turbulence model

$$\frac{\partial}{\partial t}(\alpha_i\rho_i k_i) + \nabla\cdot(\alpha_i\rho_i\boldsymbol{U}_i k_i) = \nabla\cdot\left[\alpha_i\left(\mu_i + \frac{\mu_{\mathrm{t},i}}{\sigma_{\mathrm{k}}}\right)\nabla k_i\right] + \alpha_i G_{\mathrm{k}i} - \alpha_i\rho_i\varepsilon_i + \beta\left(2\frac{\eta_{qi}}{1+\eta_{qi}}k_q - 2k_i\right) - \beta(\boldsymbol{U}_q-\boldsymbol{U}_i)\left(\frac{\mu_{\mathrm{t},q}}{\sigma_q\alpha_q}\nabla\alpha_q - \frac{\mu_{\mathrm{t},i}}{\sigma_i\alpha_i}\nabla\alpha_i\right) \tag{8}$$

$$\frac{\partial}{\partial t}(\alpha_i\rho_i\varepsilon_i) + \nabla\cdot(\alpha_i\rho_i\boldsymbol{U}_i\varepsilon_i) = \nabla\cdot\left[\alpha_i\left(\mu_i + \frac{\mu_{\mathrm{t},i}}{\sigma_\varepsilon}\right)\nabla\varepsilon_i\right] + \frac{\alpha_i\varepsilon_i}{k_i}(C_{1\varepsilon}G_{\mathrm{k}i} - C_{2\varepsilon}\rho_i\varepsilon_i) + C_{3\varepsilon}\frac{\varepsilon_i}{k_i}\left[\beta\left(2\frac{\eta_{qi}}{1+\eta_{qi}}k_q - 2k_i\right) - \beta(\boldsymbol{U}_q-\boldsymbol{U}_i)\left(\frac{\mu_{\mathrm{t},q}}{\sigma_q\alpha_q}\nabla\alpha_q - \frac{\mu_{\mathrm{t},i}}{\sigma_i\alpha_i}\nabla\alpha_i\right)\right] \tag{9}$$

where

$$\mu_{\mathrm{t},i} = C_\mu\rho_i k_i^2/\varepsilon_i \tag{10}$$

$$G_{\mathrm{k}i} = \mu_{\mathrm{t},i}\left[\nabla\boldsymbol{U}_i\cdot\left(\nabla\boldsymbol{U}_i + (\nabla\boldsymbol{U}_i)^T\right)\right] \tag{11}$$

Kinetic theory of granular flow

$$\frac{3}{2}\left[\frac{\partial}{\partial t}(\alpha_{\mathrm{s}}\rho_{\mathrm{s}}\Theta_{\mathrm{s}}) + \nabla\cdot(\alpha_{\mathrm{s}}\rho_{\mathrm{s}}\boldsymbol{U}_{\mathrm{s}}\Theta_{\mathrm{s}})\right] = (-P_{\mathrm{s}}\mathbf{I} + \boldsymbol{\tau}_s):\ \nabla\boldsymbol{U}_{\mathrm{s}} + \nabla\cdot(k_{\Theta_{\mathrm{s}}}\nabla\Theta_{\mathrm{s}}) - \gamma_{\Theta_{\mathrm{s}}} + \phi_{\mathrm{sl}} \tag{12}$$

$$P_{\mathrm{s}} = \alpha_{\mathrm{s}}\rho_{\mathrm{s}}\Theta_{\mathrm{s}}[1 + 2g_0\alpha_{\mathrm{s}}(1+e_{\mathrm{ss}})] \tag{13}$$

$$g_0 = \frac{1}{1 - \left(\alpha_{\mathrm{s}}/\alpha_{\mathrm{s,max}}\right)^{1/3}} \tag{14}$$

$$\mu_{\mathrm{s}} = \frac{10\rho_{\mathrm{s}}d_{\mathrm{p}}\sqrt{\pi\Theta_{\mathrm{s}}}}{96\alpha_{\mathrm{s}}(1+e_{\mathrm{ss}})g_0}\left[1 + \frac{4}{5}(1+e_{\mathrm{ss}})g_0\alpha_{\mathrm{s}}\right]^2 + \frac{4}{5}\alpha_{\mathrm{s}}\rho_{\mathrm{s}}d_{\mathrm{p}}(1+e_{\mathrm{ss}})g_0\sqrt{\frac{\Theta_{\mathrm{s}}}{\pi}} \tag{15}$$

$$k_{\Theta_{\mathrm{s}}} = \frac{150\rho_{\mathrm{s}}d_{\mathrm{p}}\sqrt{\Theta_{\mathrm{s}}\pi}}{384(1+e_{\mathrm{ss}})g_0}\left[1 + \frac{6}{5}\alpha_{\mathrm{s}}g_0(1+e_{\mathrm{ss}})\right]^2 + 2\alpha_{\mathrm{s}}^2\rho_{\mathrm{s}}d_{\mathrm{p}}g_0(1+e_{\mathrm{ss}})\sqrt{\frac{\Theta_{\mathrm{s}}}{\pi}} \tag{16}$$

$$\gamma_{\Theta_{\mathrm{s}}} = \frac{12\alpha_{\mathrm{s}}^2\rho_{\mathrm{s}}g_0}{d_{\mathrm{p}}}\left(1-e_{\mathrm{ss}}^2\right)\left(\frac{\Theta_{\mathrm{s}}^3}{\pi}\right)^{1/2} \tag{17}$$

$$\phi_{\mathrm{sl}} = -3\beta\Theta_{\mathrm{s}} \tag{18}$$

Johnson-Jackson wall boundary condition

$$\boldsymbol{\tau}_{\mathrm{sw}} = -\frac{\sqrt{3}}{6}\pi\rho_{\mathrm{s}}g_0\phi\frac{\alpha_{\mathrm{s}}}{\alpha_{\mathrm{s,max}}}\sqrt{\Theta}\boldsymbol{U}_{\mathrm{sw}} \tag{19}$$

$$q_{\mathrm{sw}} = \frac{\sqrt{3}}{6}\pi\rho_{\mathrm{s}}g_0\phi\frac{\alpha_{\mathrm{s}}}{\alpha_{\mathrm{s,max}}}\sqrt{\Theta}\boldsymbol{U}_{\mathrm{sw}}\cdot\boldsymbol{U}_{\mathrm{sw}} - \frac{\sqrt{3}}{4}\pi\rho_{\mathrm{s}}g_0\frac{\alpha_{\mathrm{s}}}{\alpha_{\mathrm{s,max}}}\left(1-e_{\mathrm{w}}^2\right)\Theta_{\mathrm{s}}^{3/2} \tag{20}$$

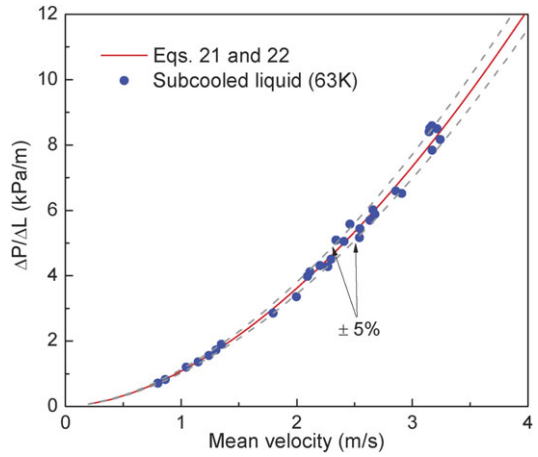

Figure 2. Pressure drop of subcooled liquid nitrogen flow.

[Color figure can be viewed in the online issue, which is available at wileyonlinelibrary.com.]

system. The comparison of the theoretical results calculated with the Darcy–Weisbach equation and the Blasius equation, that is, Eqs. 21 and 22, with the experimental results is shown in Figure 2.

$$\Delta P = f \cdot \frac{1}{2}\rho U^2 \frac{L}{D} \tag{21}$$

$$f = \frac{0.3164}{Re^{0.25}} \quad (Re < 1.0 \times 10^5) \tag{22}$$

The Reynolds number Re is defined as

$$Re = \frac{\rho UD}{\mu_l} \tag{23}$$

where the density ρ_l and the viscosity μ_l are those of subcooled liquid nitrogen (63 K). It is shown in Figure 2 that, the pressure drop of subcooled liquid nitrogen agrees well with the theoretical results with a deviation of ±5.0% when the mean velocity is from 0.8 to 3.25 m/s, indicating good reliability of the experimental system.

Pressure drop of slush nitrogen

Figure 3 presents the experimental and numerical results of the slush nitrogen flow in the horizontal pipe, compared with the data of subcooled liquid nitrogen calculated by Eqs. 21 and 22. The solid volume fraction is from 10.0 to 30.0%, and the mean velocity is in the range of 0.5–3.5 m/s in the experiments. In the case that slush density ρ_{sl} ($= \rho_s\alpha_s + \rho_l(1 - \alpha_s)$) and the viscosity μ_l of subcooled liquid nitrogen (63 K) is used, the Reynolds number ranges from 1.46×10^4 to 1.04×10^5, indicating all the flow of slush nitrogen is turbulent. In the modeling with the Eulerian–Eulerian multiphase model, the mean velocity is from 1.0 to 3.5 m/s, and the flow of slush nitrogen lower than 1.0 m/s is not modeled in the study and the reason will be given in the following context. It is shown in Figure 3 that the numerical pressure drop of slush nitrogen flow agrees well with the experimental results for all the flow conditions, and the model has high accuracy for slush nitrogen flow. The pressure drop of slush nitrogen is found always higher than that of liquid flow under the same conditions and increases with the solid volume fraction at the same mean velocity, that is to say, the solid particles have an important influence on the slush flow. Based on the fundamental assumption that the friction is confined to the boundary of a suspension flow, the frictional loss of the solid–liquid flow in a horizontal pipe is considered as a combination of the viscous friction and the mechanical friction.

Similar to the single-phase flow, the laminar sublayer is also formed over the pipe wall in the slurry flow. The lift force acting on the particles is significant in the near-wall region due to the large velocity gradient, and it repels the particles from the wall of the horizontal pipe and then a thin liquid film, namely the laminar sublayer, is formed over the pipe wall. The viscous friction is due to the liquid viscosity in the laminar sublayer, and the effect of solid particles on the viscous friction depends on the particle size. When the particles are fine enough to be trapped within the laminar sublayer, the density of the fluid in the laminar sublayer will be changed by the immersed particles. However, the particle size in slush nitrogen is about 1.0 mm, much larger than the thickness of the laminar sublayer. The coarse particles tend to move outside the laminar sublayer to escape from the large shear force in this region, and the laminar sublayer is formed entirely by liquid nitrogen, and therefore, the viscous friction of slush nitrogen flow is theoretically equal to that of the flow of subcooled liquid nitrogen (63 K) under the same conditions.

However, the real slurry flow is much more complicated due to the presence of solid particles. The particles are affected not only by the lift force that causes them to migrate toward the pipe center but also by some other actions, such as the collisions among the particles that cause them dispersed more uniformly in the liquid. Especially, when the particle collisions occur in the near-wall region, the dispersive action will impel the particles toward the pipe wall, which not only generates the additional stress against the pipe wall but also results in continuous or temporary contact of the particles with the pipe wall. And, the mechanical friction then arises from these particle–wall contacts and increases with the solid volume fraction due to the stronger particle–wall interactions.

Hence, the pressure drop of slush nitrogen flow in the horizontal pipe is higher than that of subcooled liquid nitrogen

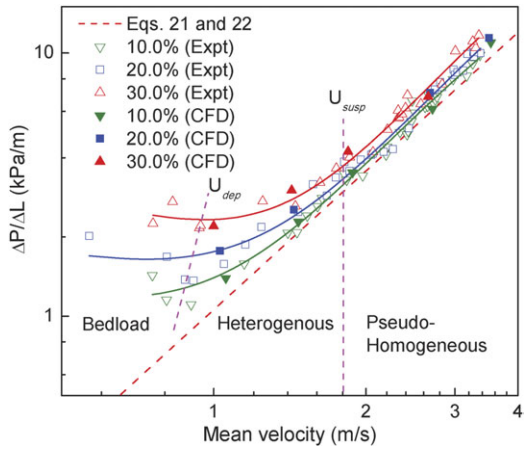

Figure 3. Experimental and numerical pressure drop of slush nitrogen flow.

[Color figure can be viewed in the online issue, which is available at wileyonlinelibrary.com.]

flow under the same conditions because of the combined action of the viscous and mechanical frictions and increases with the solid volume fraction.

Flow patterns of slush nitrogen flow

It is shown in Figure 3 that the pressure drop of subcooled liquid nitrogen changes linearly with the velocity in the logarithmic coordinates, but the dependence of the pressure drop of slush nitrogen flow on the velocity varies in different regions, which is because different flow patterns occur under the different flow conditions. As mentioned previously, the slurry flows in a horizontal pipe can be classified into four patterns based on the particle distribution on the cross-section, and due to different flow mechanisms the dependence of the pressure drop on the velocity also varies with the flow pattern. Almedeij and Algharaib[25] proposed the flow pattern diagram for the slurry flow in a horizontal pipe, according to which the experimental results of slush nitrogen given in Figure 3 can be classified into three parts: pseudo-homogeneous, heterogeneous, and bedload.

At the velocity larger than 1.8 m/s, with the corresponding Reynolds number higher than 5.16×10^4 to 5.34×10^4 at solid volume fraction of 10–30%, the pressure drop of slush nitrogen increases with the mean velocity, and the profiles of slush nitrogen at various solid volume fractions are nearly parallel to that of subcooled liquid nitrogen, which is in accord with the homogeneous flow. In the typical homogeneous flow, the particles distribute uniformly throughout the pipe cross-section due to the strong suspending forces, but the modeling results presented in Figure 4 show different features. The apparent nonuniform distributions of the particles in both horizontal and vertical directions are found at the mean velocity of 3.0 m/s and the solid volume fraction of 10.0–30.0%, namely, the Reynolds number of 8.59×10^4 to 8.91×10^4. The solid volume fraction is symmetrical about the central vertical plane of the pipe in the horizontal direction and becomes smaller while closer to the pipe wall. The distribution of solid volume fraction is more complicated in the vertical direction, and the solid volume fractions show maximum values above the bottom wall. Figure 4a shows that the solid volume fraction slightly increases with the decrease of the height in the core region and rapidly decreases in the near-wall region for all cases. The nonuniform distribution of solid particles in the core region arises from the support forces not high enough for the complete suspension of solid nitrogen particles. The large solid particles require higher support forces for the suspension,[6] namely, the higher turbulent diffusion of liquid phase and the higher particle interactions in the case of slush nitrogen flow. At the mean solid volume fraction of 10.0% where the particle interactions are very weak, the obvious nonuniformity of solid distribution in the vertical direction indicates that the turbulent diffusion, which is the dominant mechanism for particle support, is too weak to suspend the particles completely. And at the mean solid volume fractions of 20.0 and 30.0%, the gradients of the solid volume fraction profile ($|\partial\alpha_s/\partial y|$) in the core region are smaller than that at the mean solid volume fraction of 10.0% due to the stronger particle contact providing additional suspending force. The reduction of solid volume fraction in the near-wall region was also found in the experimental studies on other slurry flows.[26–28] This is because the lift force is significant in the near-wall region due to the steep velocity gradient, pushing the particles away from the pipe wall and reducing the solid volume fraction in this region.

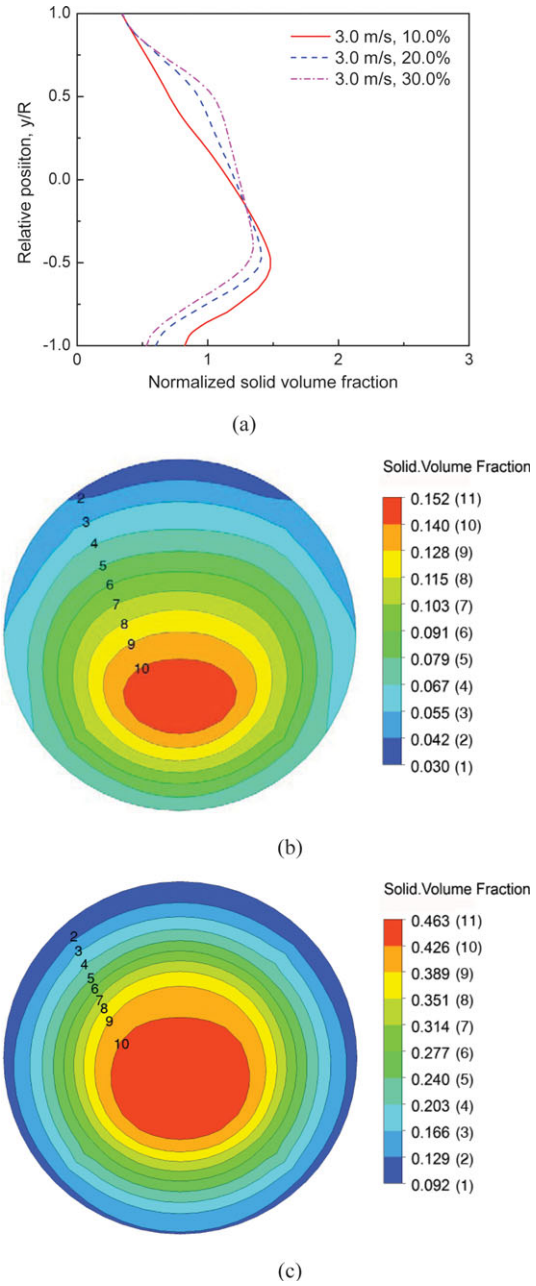

Figure 4. Numerical distributions of solid volume fraction in the pseudo-homogeneous flow (a) in the vertical direction with α_s = 10.0–30.0%, (b) at the outlet with α_s = 10.0%, and (c) at the outlet with α_s = 30.0%.

[Color figure can be viewed in the online issue, which is available at wileyonlinelibrary.com.]

The flow of slush nitrogen under this condition is described as the pseudo-homogeneous, where the flow shares the properties of the typical homogeneous flow that the dependence of the pressure drop on the mean velocity is similar to the single-phase flow, although the particle distribution is not completely uniform over the cross-section of the pipe.

When the mean velocity is in the range from about 1.0 to 1.8 m/s and the corresponding Reynolds number is from 2.86×10^4 to 5.34×10^4, the pressure drop of slush

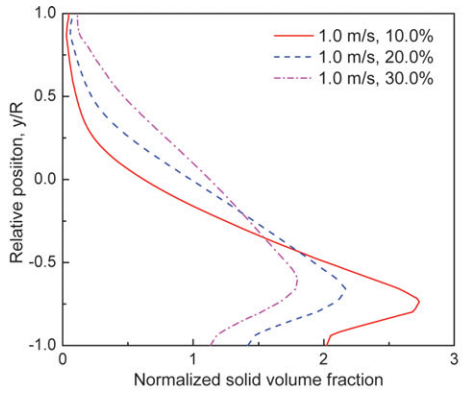

(a)

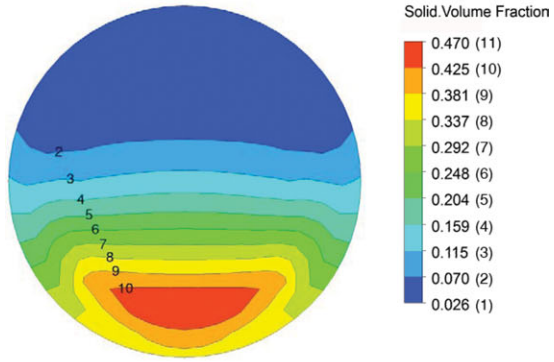

(b)

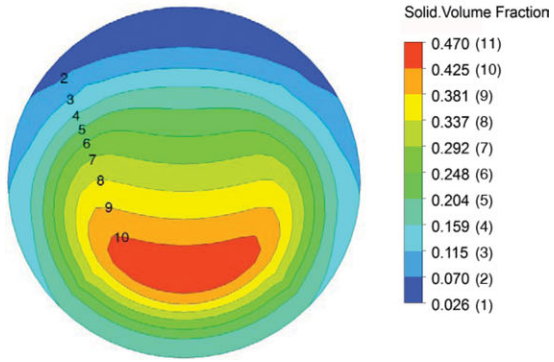

(c)

Figure 5. Numerical distributions of solid volume fraction in the heterogeneous flow (a) in the vertical direction with α_s = 10.0–30.0%, (b) at the outlet with α_s =10.0%, and (c) at the outlet with α_s = 30.0%.

[Color figure can be viewed in the online issue, which is available at wileyonlinelibrary.com.]

nitrogen still increases with the mean velocity as shown in Figure 3, but the profiles of slush nitrogen start to deviate from that of subcooled liquid nitrogen, and the divergence becomes larger as the mean solid volume fraction increases and the mean velocity decreases. The effect of solid particles on slush flow in this case is greater than that in the pseudo-homogeneous flow; and the flow pattern is determined to be the heterogeneous flow under this condition. The distributions of solid volume fraction at the mean velocity of 1.0 m/s and the solid volume fraction in the range of 10.0–30.0% obtained in the modeling are presented in Figure 5. The solid volume fraction is symmetrical in the horizontal direction and becomes smaller near the pipe wall due to the lift force, similar to that in the pseudo-homogeneous flow, but the nonuniform distribution in the vertical direction is much more significant due to the weak turbulent diffusion of liquid phase at the mean velocity of 1.0 m/s. Therefore, in the case of α_s = 10.0%, only one-tenth of solid particles are moving in the upper part of the pipe, and the other nine-tenths are moving in the lower part due to the turbulent diffusion and the particle interactions are both weak. The deposition of particles in the lower part of the pipe highly enhances the mechanical friction between slush nitrogen and the pipe wall, and thus, the pressure drop of slush nitrogen is significantly higher than that of subcooled liquid nitrogen. As the mean solid volume fraction increases to 20.0 and 30.0%, the stronger particle contact provides higher suspending force for the particles, and therefore, the nonuniformity of the solid volume fraction in the vertical direction decreases. The obviously different solid distributions result in the pressure drop of slush nitrogen considerably varying with the mean solid volume fraction. In addition, the sedimentation of solid particles also causes the asymmetrical distribution of the velocity about the pipe central axis, as shown in Figure 6, because more particles in the lower part of the pipe hinder the slush flow and reduce the velocity in this region. The effect of the lift force on the particle distribution is also significant at the mean velocity of 1.0 m/s, and the apparent reduction of solid volume fraction near the bottom is found for all cases in Figure 5a. The position where the solid volume fraction reaches the maximum is farther away from the bottom wall at the higher mean solid volume fraction, that is to say, the lift force increases with the solid volume fraction, which is in accordance with the model of the lift force given in Eq. 2. The numerical results of slush nitrogen flow at the mean velocity of 1.0 m/s indicate that the flow belongs to the typical heterogeneous flow, in agreement with the experimental results.

In the heterogeneous flow, the pressure drop of slush nitrogen decreases with the mean velocity until it approaches the minimum value, and then starts to increase as the mean velocity further decreases, which is contrary to the single-phase flow. And the flow under this condition is the bedload

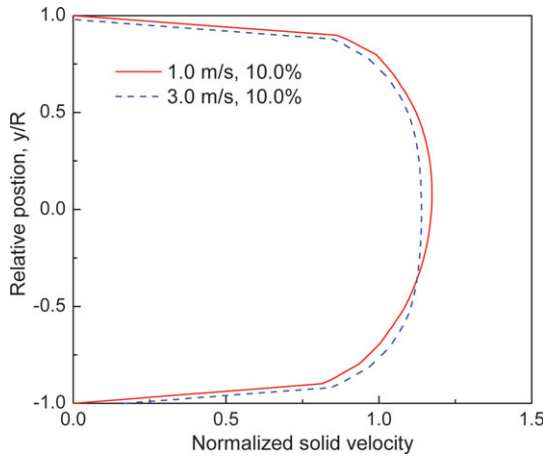

Figure 6. Numerical solid velocity profiles in the vertical direction of slush nitrogen flow.

[Color figure can be viewed in the online issue, which is available at wileyonlinelibrary.com.]

flow, where the turbulent diffusion is too weak to move all the particles. Some of the particles are suspended in the liquid and move in the upper part of the pipe as a heterogeneous flow, and the others accumulate and form a bed layer at the bottom. In the bed layer, the particle contact instead of the turbulent diffusion becomes the dominant mechanism for particle support, and the different mechanism causes the Eulerian–Eulerian multiphase model inappropriate anymore and therefore, the bedload flow is not modeled in this study. The sediment particles roll and slide near the pipe wall, highly increasing the mechanical friction, and the friction grows larger at the lower velocity, because more particles deposit at the bottom. Hence, the pressure drop of slush nitrogen in the bedload flow increases, as the mean velocity decreases, as shown in Figure 3.

In general, the bedload flow includes the moving-bed flow and the stationary-bed flow on the basis of the behavior of the bed layer. However, the flow pulsations are often observed at the low velocity in the experiments, indicating that the stable bed layer is difficult to form in the slush nitrogen flow. The pipe in this study has the inner diameter of 10.0 mm, relatively small for the slush nitrogen with the particles of 1.0 mm. When the bed layer forms at the pipe bottom, the region for the suspending flow in the upper part is significantly reduced, and the flow of the coarse particles will be hindered, resulting in the pipe chocked very easily. Figure 7 presents the measured pressure drop under different conditions, and the amplitude of fluctuation of the pressure drop at 0.9 m/s, 10.0% and 0.83 m/s, 30.0% is up to 5.0 kPa/m, which is nearly three times as high as that at 2.67 m/s, 10.0% and 2.4 m/s, 30.0%, indicating the flow pulsation occurs at the very low velocity. As no stable bed layer forms in slush nitrogen flow, the bedload flow pattern instead the moving-bed or the stationary-bed flows is concluded in this study.

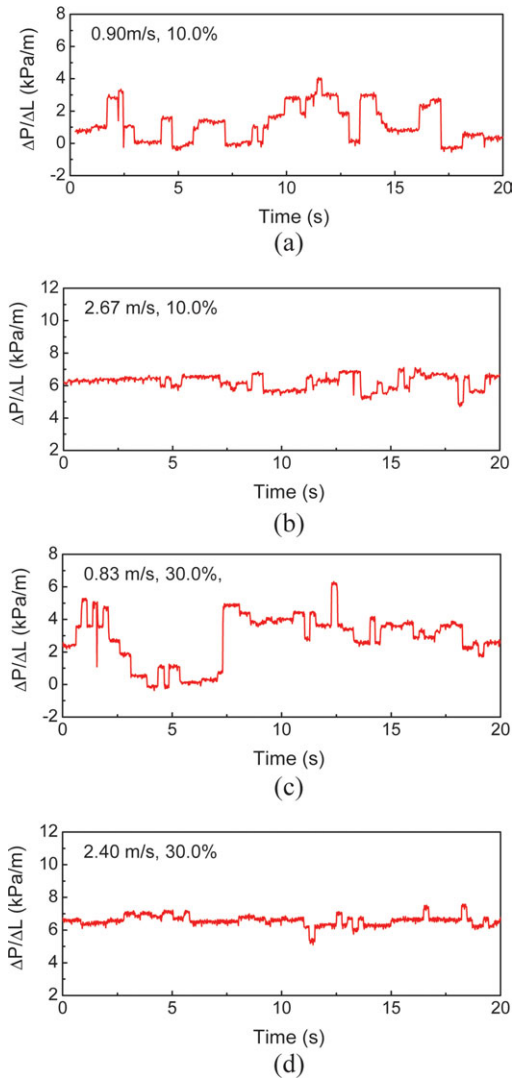

Figure 7. Fluctuation of the measured pressure drop of slush nitrogen under various flow conditions.

(a) U = 0.90 m/s, α_s = 10.0%, (b) U = 2.67 m/s, α_s = 10.0%, (c) U = 0.83 m/s, α_s = 30.0%, and (d) U = 2.40 m/s, α_s = 30.0%. [Color figure can be viewed in the online issue, which is available at wileyonlinelibrary.com.]

Transition velocities

Two transition velocities between the flow patterns of slush nitrogen flow in a horizontal pipe are discussed in this study. One is the suspending velocity U_{susp}, above which the slurry flow behaves in the homogeneous fashion, in other words, the pressure drop profiles of slurry flow are parallel to that of the liquid flow in the flow pattern diagram. As shown in Figure 3, the suspending velocity for slush nitrogen flow in the horizontal pipe of 10.0 mm in diameter is taken as U_{susp} = 1.8 m/s. Newitt et al.[29] proposed the following equation to estimate the suspending velocity

$$U_{susp} = \sqrt[3]{1800 g D U_t} \tag{24}$$

U_t is the terminal velocity of the particles under free settling and is calculated by the Cheng equation,[30] formulated as

$$U_t = \frac{\mu_l}{\rho_l d_p}\left(\sqrt{25 + 1.2 d_{p^*}^2} - 5\right)^{1.5} \tag{25}$$

where the dimensionless particle diameter d_{p^*} is defined as

$$d_{p^*} = \left[\frac{(\rho_s/\rho_l - 1)\rho_l^2 g}{\mu_l^2}\right]^{1/3} d_p \tag{26}$$

The Cheng equation is suitable for a wide range of the particle Reynolds number, from Stokes to turbulent flow. The suspending velocity is affected by the particle size, the pipe diameter, and the properties of two phases, but independent of the solid volume fraction. For slush nitrogen flow in this study, the suspending velocity calculated by the Newitt equation is U_{susp} = 1.87 m/s, very close to the value 1.80 m/s obtained in the experiments.

The other one is the limit deposit velocity U_{dep} between the heterogeneous flow and the bedload flow. As mentioned previously, as the velocity decreases the pressure drop of slush nitrogen flow decreases in the heterogeneous flow until it reaches a minimum, and then increases with the decrease of the velocity, and the flow is changed into the bedload flow. The critical velocity at the minimal pressure drop of slush nitrogen flow is the limit deposit velocity, which is determined to be 0.89–0.94 m/s for the solid volume fraction of 10.0–30.0% according to the flow diagram presented in Figure 3. Many empirical and theoretical correlations have

Table 2. Limit Deposit Velocity of Slurry Flow in the Literature

Literature	Model Equation	
Durand and Condolios[31]	$U_{dep} = F_L\sqrt{2gD(SG-1)}\ \ (F_L = 1.3)$	(27)
Newitt et al.[29]	$U_{dep} = 34/\sqrt{3C_{D,dep}}$	(28)
Wasp et al.[32]	$U_{dep} = F_{L'}(d_p/D)^{-1/3}\ \ (F_{L'} = 3.4\alpha_s^{0.22})$	(29)
Zandi and Govatos[33]	$U_{dep} = \left[40\alpha_s gD(SG-1)/\sqrt{C_{D,dep}}\right]^{1/2}$	(30)
	$C_{D,dep} = 4gd_p(SG-1)/(3U_t^2)$	(31)

been proposed for the limit deposit velocity, and some of them, including Durand–Condolios,[31] Newitt et al.[29] Wasp et al.[32] and Zandi–Govatos[33] correlations, are summarized in Table 2. It should be noted that the drag coefficient $C_{D,dep}$ in the Newitt and the Zandi–Govatos correlations is calculated by Eq. 31 instead of the Gidaspow drag model used in the modeling, because the slip velocity between two phases $|\boldsymbol{U}_l - \boldsymbol{U}_s|$ used in Eq. 7 is unable to be determined in the experiment.

Figure 8 presents the comparison between the experimental limit deposit velocity and the calculated values with the correlations given in Table 2. The experimental results are considerably higher than all the theoretical values calculated by the correlations, and this probably arises from the small pipe diameter and the large particles in slush nitrogen flow. The correlations given in Table 2 were generally obtained from the slurry flows in the pipe with the diameter range from dozens of to hundreds of millimeters. The limit deposit velocity of slurry flow is considered to increase with the pipe diameter,[6] but this is concluded from the slurry flow with the pipe diameter of 50–100 mm where the moving-bed and the stationary-bed flows can be formed. However, for slush nitrogen flow, as the pipe is easily chocked due to the narrow pipe and the coarse particles as stated previously, causing the flow pulsation at the higher velocity and increasing the pressure drop. In this study, the limit deposit velocity is determined from the dependence of the pressure drop on the mean velocity, and therefore, it is reasonable that the experimental limit deposit velocity of slush nitrogen flow is higher than the predicted values by these correlations.

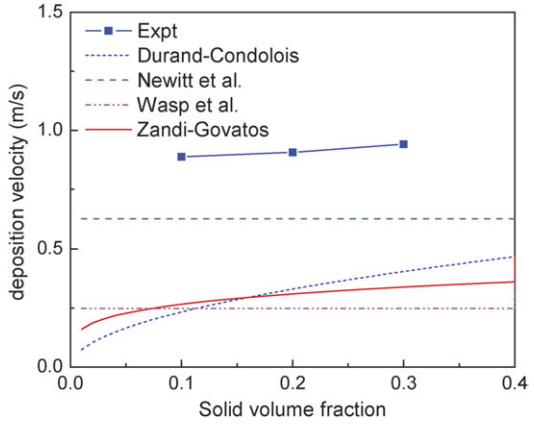

Figure 8. Comparison of the experimental and theoretical deposit velocities for slush nitrogen flow.

[Color figure can be viewed in the online issue, which is available at wileyonlinelibrary.com.]

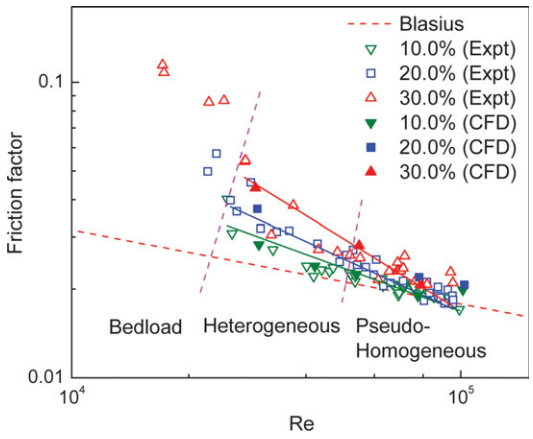

Figure 9. Variation of the friction factor with the Reynolds number for the slush nitrogen flow.

The solid lines shown in the figure are the fitting curves to the data in pseudohomogeneous and heterogeneous flows. [Color figure can be viewed in the online issue, which is available at wileyonlinelibrary.com.]

Friction factor of slush nitrogen

Variation of the friction factor with the Reynolds number of slush nitrogen flow is presented in Figure 9, where the slush density ρ_{sl} and the viscosity of the liquid nitrogen at the triple point μ_l are used in the calculation. The numerical results for slush nitrogen flow with various solid volume fractions are in good agreement with the experimental results. The friction factor of slush nitrogen is higher than that of the liquid flow at the same Reynolds number due to the presence of solid particles. At the low Reynolds number where the bedload flow occurs, the friction factor of slush nitrogen is nearly 4.0 times of that of the liquid flow, because the particle sedimentation at the pipe bottom enhances the mechanical friction of slush flow. In the heterogeneous and the pseudo-homogeneous flow, the effect of solid particles is much lower than that in the bedload flow and decreases with the increase of the Reynolds number, and the friction factor of the slush nitrogen flow is much close to that of the liquid nitrogen flow at the Reynolds number range of 8×10^4 to 1×10^5.

The difference of the friction factor among various mean solid volume fraction is considerable, as shown in Figure 9. To obtain the general *f–Re* relationship that takes the effect of solid particles into account, the Reynolds number is modified by replacing the liquid nitrogen viscosity μ_l with the effective viscosity of slush nitrogen μ_{sl}, and the modified Reynolds number is described as slush Reynolds number Re_{sl}

$$Re_{sl} = \frac{\rho_{sl}UD}{\mu_{sl}} \tag{32}$$

Some of the equations for the effective viscosity of slurry flow are given in Table 3, where μ_r $(=\mu_{sl}/\mu_l)$ is the relative viscosity defined as the ratio of the slush effective viscosity to the

Table 3. Relative Viscosity of Slurry Flow in the Literature

Literature	Model Equation	
Einstein[34]	$\mu_r = 1 + 2.5\alpha_s$	(33)
Thomas[35]	$\mu_r = 1 + 2.5\alpha_s + 10.05\alpha_s^2 + 0.00273\exp(16.6\alpha_s)$	(34)
Orr and Dalla Valle[36]	$\mu_r = (1 - \alpha_s/0.6)^{-1.8}$	(35)
Mori and Ototake[37]	$\mu_r = 1 + 3\left(\alpha_s^{-1} - \alpha_{s,max}^{-1}\right)^{-1}$	(36)

liquid-phase viscosity. In the Einstein equation,[34] the relative viscosity of slurry flow is considered proportional to the solid volume fraction, and the effect of the particle size and the particle interactions are not taken into account, and therefore, it is usually applied to the dilute slurry flows. Another frequently applied model is the Thomas equation,[35] which is valid for the spherical particles with the solid volume fraction up to 62.5%, and the coefficient of 2.5 is known dependent on the particle aspect ratio, and the terms of the order higher than unity are attributed to the particle interactions effects. Additionally, Orr–DallaValle equation[36] and Mori–Ototake equation,[37] which were utilized in the investigation on slush nitrogen in a horizontal pipe by Ohira[5] and Matsuo et al.,[3] respectively, are also discussed in this study. It is found that the relative viscosities of slush nitrogen calculated by various equations are very close at the solid volume fraction lower than 10.0%. At the higher solid volume fraction, the relative viscosity obtained by Einstein equation is proportional to the solid volume fraction, but the values obtained by the other three equations increase rapidly. As the solid volume fraction ranging from 0 to 30.0%, the relative viscosities calculated by the Thomas, the Orr–DallaValle, and Mori–Ototake equations are very close, only the Einstein equation and the Thomas equation are compared in this study.

The experimental data are reanalyzed with the Einstein equation and the Thomas equation, respectively, and the results are presented in Figure 10. It is found that the friction factors vs. the slush Reynolds number for various solid volume fractions are generalized when the Einstein equation is used. But in the case of the Thomas equation, the obvious divergence among the results with different solid volume fractions still exists, although it is smaller than that in the case when the liquid viscosity is used in Figure 9. It is indicated that the Einstein equation is more appropriate to slush nitrogen than the Thomas equation. It should be noticed that the Einstein equation is generally applicable to the dilute slurry flow as mentioned previously. The better agreement of the Einstein equation and the experimental results with the solid volume fraction up to 30.0% indicates that the effective viscosity of slush nitrogen is reduced by some factors, but on the basis of the results obtained so far these factors are difficult to be identified. As the deeper research and the development of the measurement technology, more work on this issue is expected to be done in the future.

The friction factor vs. the slush Reynolds number for slush nitrogen can be obtained by the least square method as

$$f = \frac{5.978}{Re_{sl}^{0.5224}} \quad (1.7 \times 10^4 < Re_{sl} < 8.1 \times 10^4) \tag{37}$$

In the above equation, only the data in the heterogeneous and the pseudo-homogeneous flows are used for the fitting because of the different flow mechanism in the bedload flow. Figure

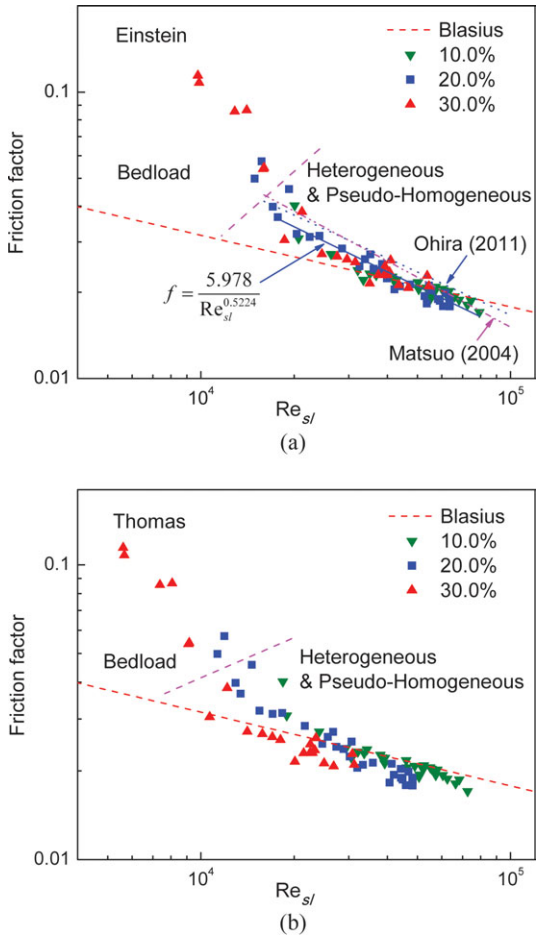

Figure 10. Variation of the friction factor with the slush Reynolds number for slush nitrogen flow.

(a) Einstein equation and (b) Thomas equation. [Color figure can be viewed in the online issue, which is available at wileyonlinelibrary.com.]

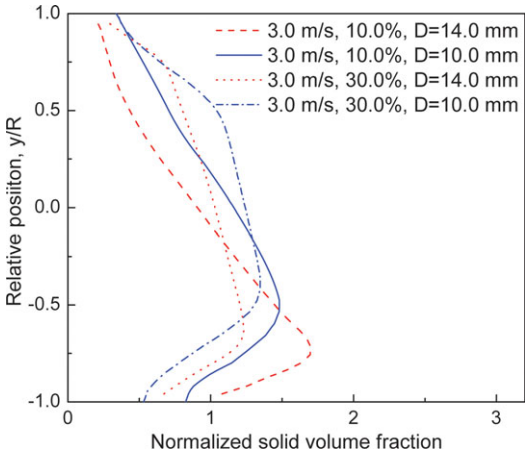

Figure 11. Numerical distributions of solid volume fraction of slush nitrogen flow in the horizontal pipes with the diameter of 14.0 and 10.0 mm.

[Color figure can be viewed in the online issue, which is available at wileyonlinelibrary.com.]

10a also presents the results by Ohira[5] and Matsuo et al.,[3] which are expressed as Eqs. 38 and 39, respectively.

$$f = \frac{5.263}{Re_{sl}^{0.5}} \quad (2.35 \times 10^4 < Re_{sl} < 1.69 \times 10^5) \tag{38}$$

$$f = \frac{12}{Re_{sl}^{0.58}} \quad (5 \times 10^3 < Re_{sl} < 1 \times 10^5) \tag{39}$$

The friction factor of slush nitrogen flow obtained in the experiments is slightly lower than that from the literature at the same slush Reynolds number, which is considered to arise from the different pipe diameters. The inner diameter of the pipe is 15.0 mm in Ohira,[5] 14.0 mm in Matsuo et al.,[3] and 10.0 mm in this study. The comparison of the numerical distributions of slush volume fraction in the vertical direction presented in Figure 11 indicates that the migration of solid particles toward the pipe center is stronger with the pipe diameter of $D = 10.0$ mm than that with the pipe diameter of $D = 14.0$ mm, and this may decrease the additional stress against the pipe wall generated by the particle–particle collisions in the near-wall region, and furthermore decrease the friction between slush nitrogen and the pipe wall. However, the discrepancy between the results of this study and from the literature is not significant, and therefore, the effect of the additional stress on slush nitrogen flow is small.

Conclusions

In this study, the flow characteristics of slush nitrogen in a horizontal pipe with the inner diameter of 10.0 mm are studied experimentally and theoretically. When the mean velocity ranges from 0.5 to 3.5 m/s and the mean solid volume fraction is up to 30.0%, the pressure drop per unit length of slush nitrogen is always higher than that of subcooled liquid nitrogen under the same condition, because the viscous friction and the mechanical friction both occur in slush nitrogen flow. And the pressure drop increases with the solid volume fraction due to the higher mechanical friction at the higher solid volume fraction. On the basis of the experimental and theoretical results, three flow patterns of slush nitrogen are determined: pseudo-homogeneous, heterogeneous, and bedload. In the pseudo-homogeneous flow, the particles are distributed slightly nonuniformly on the cross-section due to the coarse particles in slush nitrogen and the pressure drop changes linearly with the mean velocity in the logarithmic coordinates. In the case of the heterogeneous flow, obvious gradients are found in the solid volume fraction profiles for all the flows, and the divergence between the pressure drop of the slush and liquid flow increases as the mean velocity decreases. In the bedload flow, the sedimentation of particles significantly increases the pressure drop of slush nitrogen flow, and the flow pulsations are also found in the experiments, indicating the great instability of the flow. The transition velocities for slush nitrogen flow are determined as $U_{susp} = 1.8$ m/s and $U_{dep} = 0.89$–0.94 m/s with the solid volume fraction of 10.0–30.0%. Due to the application of the effective viscosity, the general correlation of the friction factor with the slush Reynolds number of slush nitrogen with various solid volume fractions is obtained.

Acknowledgments

This research is jointly supported by the National Natural Science Foundation of China under Contact No. 50976068 and the Fok Ying-Tung Education of China under Contact No. 121056.

Notation

C_μ, $C_{1\varepsilon}$, $C_{2\varepsilon}$, $C_{3\varepsilon}$ = empirically assigned constants in turbulence model
C_D = drag coefficient of a particle
$C_{D,dep}$ = drag coefficient used in limit deposit velocity
C_L = lift coefficient
C_{VM} = virtual mass coefficient
D = pipe diameter, m
d_p = particle diameter, m
e_{ss} = particle–particle restitution coefficient
e_w = particle–wall restitution coefficient
f = friction factor
G_k = production of turbulent kinetic energy
$\boldsymbol{g}$ = gravitational acceleration, m/s^2
g_0 = radial distribution function
$\mathbf{I}$ = unit tensor
I = turbulence intensity
k = turbulence kinetic energy, m^2/s^2
k_{Θ_s} = diffusion coefficient of granular temperature
L = pipe length, m
P = pressure, Pa
Re = Reynolds number
Re_p = particle Reynolds number
Re_{sl} = slush Reynolds number
$\boldsymbol{U}$ = velocity, m/s

Greek Letters

α = volume fraction
β = drag coefficient, kg/(m^3 s)
ϕ = specularity coefficient
Θ_s = granular temperature, m^2/s^2
ε = dissipation rate of turbulent kinetic energy, m^2/s^3
λ_s = solid bulk viscosity, Pa s
μ = viscosity, Pa s
ρ = density, kg/m^3
γ_{Θ_s} = collisional dissipation of energy, kg/(m^3 s)
$\boldsymbol{\tau}$ = viscous stress tensor, Pa
ϕ_{sl} = fluctuating energy exchange between two phases, kg/(m^3 s)
σ_k, σ_ε, σ_{sl} = turbulent Prandtl numbers

Subscripts

l = liquid
s = solid
sl = slurry
t = turbulent

Literature Cited

1. Sindt CF. A summary of the characterization study of slush hydrogen. *Cryogenics*. 1970;10:372–380.
2. Carney RR. Slush hydrogen production and handling as a fuel for space projects. *Adv Cryog Eng*. 1964;9:529–536.
3. Matsuo K, Ikeuchi M, Machida A, Yasuda K. Fundamental study of pipe flow and heat transfer characteristics of slush nitrogen. *Adv Cryog Eng*. 2006;51:1033–1040.
4. Sindt CF, Ludtke PR. Slush hydrogen flow characteristics and solid fraction upgrading. *Adv Cryog Eng*. 1970;15:382–390.
5. Ohira K. Pressure drop reduction phenomenon of slush nitrogen flow in a horizontal pipe. *Cryogenics*. 2011;51:389–396.
6. Doron P, Barnea D. Flow pattern maps for solid–liquid flow in pipes. *Int J Multiphase Flow*. 1996;22:273–283.
7. Takakoshi T, Murakami M, Ikeuchi M, Matsuo K, Tsukahara R. PIV measurement of slush nitrogen flow in a pipe. *Adv Cryog Eng*. 2006;51:1025–1032.
8. Ishimoto J, Ono R. Numerical study of the two-phase flow characteristics of slush nitrogen. *Cryogenics*. 2005;45:304–316.
9. Gao D, Herbst JA. Alternative ways of coupling particle behaviour with fluid dynamics in mineral processing. *Int J Comput Fluid D*. 2009;23:109–118.
10. Ohira K, Ota A, Mukai Y, Hosono T. Numerical study of flow and heat-transfer characteristics of cryogenic slush fluid in a horizontal circular pipe (SLUSH-3D). *Cryogenics*. 2012;52:428–440.
11. Jiang YY, Zhang P. Numerical investigation of slush nitrogen flow in a horizontal pipe. *Chem Eng Sci*. 2012;73:169–180.

12. Savage SB, Jeffrey DJ. The stress tensor in a granular flow at high shear rates. *J Fluid Mech*. 1981;110:255–272.
13. Jenkins JT, Savage SB. A theory for the rapid flow of identical, smooth, nearly elastic, spherical particles. *J Fluid Mech*. 1983;130: 187–202.
14. Lun CKK, Savage SB, Jeffrey DJ, Chepurniy N. Kinetic theories for granular flow: inelastic particles in Couette flow and slightly inelastic particles in a general flowfield. *J Fluid Mech*. 1984;140:223–256.
15. Louge MY, Mastorakos E, Jenkins JT. Role of particle collisions in pneumatic transport. *J Fluid Mech*. 1991;231:345–359.
16. Bolio EJ, Yasuna JA, Sinclair JL. Dilute turbulent gas–solid flow in risers with particle–particle interactions. *AIChE J*. 1995;41:1375–1388.
17. Cornelissen JT, Taghipour F, Escudié R, Ellis N, Grace JR. CFD modelling of a liquid–solid fluidized bed. *Chem Eng Sci*. 2007; 62:6334–6348.
18. Jiang YY, Zhang P. Density determination of slush nitrogen by the improved capacitance-type densimeter. *Exp Therm Fluid Sci*. 2011;35:328–337.
19. Gidaspow D, Bezburuah R, Ding J. *Hydrodynamics of circulating fluidized beds: kinetic theory approach*. In: *Fluidization VII, Proceedings of the 7th Engineering Foundation Conference on Fluidization*, Gold Coast, Australia. New York: AIChE, 1992;75–82.
20. Arnold GS, Drew DA, Lahey RT. Derivation of constitutive equations for interfacial force and Reynolds stress for a suspension of spheres using ensemble cell averaging. *Chem Eng Commun*. 1989;86:43–54.
21. Drew DA, Passman SL. *Theory of Multicomponent Fluids*. New York: Springer, 1999.
22. Barnes HA, Hutton JF, Walters K. *An Introduction to Rheology*. Amsterdam: Elsevier, 1989.
23. Johnson PC, Jackson R. Frictional-collisional constitutive relations for granular materials, with application to plane shearing. *J. Fluid Mech*. 1987;176:67–93.
24. Benyahia S, Syamlal M, O'Brien TJ. Study of the ability of multiphase continuum models to predict core-annulus flow. *AIChE J*. 2007;53:2549–2568.
25. Almedeij JH, Algharaib MK. Influence of sand production on pressure drawdown in horizontal wells: theoretical evidence. *J Petrol Sci Eng*. 2005;47:137–145.
26. Shook CA, Daniel SM, Scott JA, Holgate JP. Flow of suspensions in pipelines. Part 2: Two mechanisms of particle suspension. *Can J Chem Eng*. 1968;46:238–244.
27. Campbell CS, Avila-Segura F, Liu Z. Preliminary observations of a particle lift force in horizontal slurry flow. *Int J Multiphase Flow*. 2004;30:199–216.
28. Kaushal DR, Tomita Y. Experimental investigation for near-wall lift of coarser particles in slurry pipeline using γ-ray densitometer. *Powder Technol*. 2007;172:177–187.
29. Newitt DM, Richardson JF, Abbott M, Turtle RB. Hydraulic conveying of solids in horizontal pipes. *Trans Inst Chem Eng*. 1955;33:93–113.
30. Cheng N-S. Simplified settling velocity formula for sediment particle. *J Hydraul Eng*. 1997;123:149–152.
31. Durand R, Condolios E. Communication de R. Durand et E. *Condolios*. In: Societe Hydrotechnique de France, editor. *Compte Rendu des Deuxiemes Journees de L'Hydraulique*. Paris: La Houille Blanche, 1952;29–55.
32. Wasp EJ, Kenny JP, Gandhi RL. *Solid–Liquid Flow. Slurry Pipeline Transportation*. Clausthal: Trans Tech Publications, 1977.
33. Zandi I, Govatos G. Heterogeneous flow of solids in pipelines. *J Hydraul Div*. 1967;93:145–159.
34. Einstein A. Zur Theorie der Brownschen Bewegung. *Ann Phys (Berlin)*. 1906;324:371–381.
35. Thomas DG. Transport characteristics of suspension: VIII. A note on the viscosity of Newtonian suspensions of uniform spherical particles. *J Colloid Sci*. 1965;20:267–277.
36. Orr C, Dalla Valle JM. Heat transfer properties of liquid–solid suspensions. *Chem Eng Prog Symp Ser*. 1954;50:29–45.
37. Mori Y, Ototake N. On the viscosity of suspensions. *Kagaku Kougaku*. 1956;20:488–494 (in Japanese).

Manuscript received May 19, 2012, and revision received Aug. 2, 2012.